

Supplementary Information

Donor- π -Acceptor Heterojunctions Constructed from rGO Network and Redox-Active Covalent Organic Framework for High-Performance Supercapacitors

An-Qi Zhang,^{[a]‡} Pan Ran,^{[a]‡} Xiao Han,^[a] Si-Wen Ke,^[a] Ao-qian Qiu,^[a] Ze-Dong Zhang,^[a] Yang Lv,^[a] Meng-Ning Ding,^{[a]} Jing-Lin Zuo.^{*[a]}*

[a] A. Zhang, P. Ran, X. Han, S. Ke, A. Qiu, Z. Zhang, Y. Lv, Prof. Dr. M. Ding, Prof. Dr. J. Zuo
State Key Laboratory of Coordination Chemistry, Key Laboratory of Mesoscopic Chemistry of MOE, School of Chemistry and
Chemical Engineering
Nanjing University
Nanjing 210023, P. R. China
E-mail: zuojl@nju.edu.cn; mding@nju.edu.cn;

Characterizations

The powder X-ray diffraction (PXRD) spectra were recorded on a Bruker Advance D8 (40 kV, 40 mA) diffractometer with Cu radiation ($\lambda = 1.54056 \text{ \AA}$) at room temperature. Diffraction intensity data for 2θ from $3 \sim 30^\circ$ were collected at a scanning speed of 2 deg min^{-1} with a 2θ step increment of 0.05° . TEM images were obtained on a JEOL JEM-2100 microscope at an accelerating voltage of 200 kV. Fourier transform infrared (FTIR) spectra of the starting materials and COF samples were recorded on a Tensor II Bruker Spectrophotometer in the $4000\text{-}400 \text{ cm}^{-1}$ region. The UV-vis-NIR absorption spectra of COFs were recorded on a UV-3600 spectrophotometer. The surface morphology of the catalysts was collected using high-resolution thermal field emission scanning electron microscopy (SEM, JSM-7600 F) with an acceleration voltage of 10 kV. Gas adsorption/desorption isotherms were measured using ASAP 2020 (Micromeritics Instrument Corp USA). Thermogravimetric analysis (TGA) traces for COF samples were collected on a Perkin-Elmer TGA 4000 thermal analysis system under an air atmosphere with a flow rate of 20 ml min^{-1} from $30 \text{ }^\circ\text{C}$ to $800 \text{ }^\circ\text{C}$ with a ramp rate of $5 \text{ }^\circ\text{C min}^{-1}$.

Synthesis of 4-(4-(5,5-dimethyl-1,3-dioxan-2-yl)phenyl)-1,3-dithiole-2-thione (1).

1,3-dithiole-2-thione (1.34 g, 10.0 mmol) was dissolved in anhydrous THF (20 mL). $\text{TMPMgCl}\cdot\text{LiCl}$ (9.91 mL, 11.0 mmol, 1.11 M in THF) was added dropwise at $-78 \text{ }^\circ\text{C}$, and the mixture was stirred for 0.5 h. A ZnCl_2 solution (12.0 mL, 12.0 mmol, 1.0 M in THF) was added at $-78 \text{ }^\circ\text{C}$, and the mixture was stirred for 15 min. The freshly prepared zinc reagent was added to a solution of 2-(4-iodophenyl)-5,5-dimethyl-1,3-dioxane (2.55 g, 8.0 mmol) and $\text{Pd}(\text{PPh}_3)_4$ (1.15 g, 1.0 mmol) in anhydrous NMP (10 mL) at $25 \text{ }^\circ\text{C}$. The mixture was stirred at $25 \text{ }^\circ\text{C}$ for 24 h, then quenched with saturated aqueous NH_4Cl solution (50 mL) and extracted with EtOAc ($3 \times 100 \text{ mL}$), and the combined extracts were dried (anhydrous Na_2SO_4). After filtration, the solvents were evaporated in vacuo. The crude product was purified by flash column chromatography (isohexane/ CH_2Cl_2 (1:2); silica gel, 200-300 mesh), yielding 1 (1.78 g, 54%) as a yellow solid. $^1\text{H NMR}$ (400 MHz, CDCl_3/TMS , d/ppm, J/Hz) δ : 7.57 (d, $J = 8.0 \text{ Hz}$,

2H), 7.42 (d, $J = 8.0$ Hz, 2 H), 7.11 (s, 1H), 5.41 (s, 1H), 3.78 (d, $J = 8.0$ Hz, 2 H), 3.66 (d, $J = 8.0$ Hz, 2 H), 1.29 (s, 3H), 0.81 (s, 3H). ESI-MS (+): m/z 325.47 $[M+H]^+$.

Synthesis of 4-(4-(5,5-dimethyl-1,3-dioxan-2-yl)phenyl)-1,3-dithiole-2-thione (2).

1 (0.81 g, 2.5 mmol) was dissolved in anhydrous THF (20 mL). $TMPMgCl \cdot LiCl$ (2.48 mL, 4.4 mmol, 1.11 M in THF) was added dropwise at -78 °C, and the mixture was stirred for 0.5 h. A $ZnCl_2$ solution (4.8 mL, 4.8 mmol, 1.0 M in THF) was added at -78 °C, and the mixture was stirred for 15 min. The freshly prepared zinc reagent was added to a solution of 2-(4-iodophenyl)-5,5-dimethyl-1,3-dioxane (1.0 g, 3.2 mmol) and $Pd(PPh_3)_4$ (0.29 g, 0.25 mmol) in anhydrous NMP (10 mL) at 25 °C. The mixture was stirred at 25 °C for 24 h, then quenched with saturated aqueous NH_4Cl solution (50 mL) and extracted with EtOAc (3×100 mL), and the combined extracts were dried (anhydrous Na_2SO_4). After filtration, the solvents were evaporated in vacuo. The crude product was purified by flash column chromatography (isohexane/ CH_2Cl_2 (1:2); silica gel, 200-300 mesh), yielding 2 (1.05 g, 82%) as a yellow solid. 1H NMR (400 MHz, $CDCl_3/TMS$, d/ppm, J/Hz) δ : 7.43 (d, $J = 8.0$ Hz, 2H), 7.21 (d, $J = 8.0$ Hz, 2 H), 5.34 (s, 1H), 3.76 (d, $J = 12$ Hz, 2 H), 3.64 (d, $J = 12$ Hz, 2 H), 1.27 (s, 3H), 0.79 (s, 3H). ESI-MS (+): m/z 515.71 $[M+H]^+$.

Synthesis of 4,5-bis(4-(5,5-dimethyl-1,3-dioxan-2-yl)phenyl)-1,3-dithiol-2-one (3).

$Hg(OAc)_2$ (1.91 g, 6.0 mmol) was added portion wise to a solution of 2 (1.02 g, 2.0 mmol) in $CHCl_3$ (40 mL) and AcOH (12.5 mL) at 25 °C. The mixture was stirred at this temperature for 6 h, and the precipitate was then filtered through Celite. The resulting solution was washed with saturated aqueous Na_2CO_3 (2×100 mL) and water (2×100 mL). The organic layer was dried (anhydrous Na_2SO_4), and after filtration, the solvents were evaporated in vacuo. The crude product was purified by flash column chromatography (CH_2Cl_2 ; silica gel, 200-300 mesh), yielding 3 (0.95 g, 95%) as a colorless solid. 1H NMR (400 MHz, $CDCl_3/TMS$, d/ppm, J/Hz) δ : 7.40 (d, $J = 8.0$ Hz, 2H), 7.22 (d, $J = 8.0$ Hz, 2 H), 5.33 (s, 1H), 3.76 (d, $J = 12$ Hz, 2 H), 3.63 (d, $J = 12$ Hz, 2 H), 1.27 (s, 3H), 0.79 (s, 3H). ESI-MS (+): m/z 499.65 $[M+H]^+$.

Synthesis of bis[1,2-di(4-(5,5-dimethyl-1,3-dioxane-2-yl)phenyl)ethylene-1,2-dithiolate] nickel complex (4). 3 (1.99 g, 4 mmol) was added to a sodium methoxide solution (432 mg, 8 mmol, 20 mL). After 45 min of stirring, NiCl₂·6H₂O (1.92 g, 8 mmol) was added. Two hours later, tetrabutylammonium iodide (1.48 g, 4 mmol) was added. A black precipitate appeared immediately from the brown solution. On completion, methanol was evaporated, and the residue was diluted with dichloromethane. Excess I₂ was added to the above solution of CH₂Cl₂. The mixture was stirred for 15 min and filtered. The solvent was evaporated in a vacuum. The crude product was purified by flash column chromatography (CH₂Cl₂; silica gel, 200-300 mesh), yielding 4 (120 mg, 6%) as a green solid. ¹H NMR (400 MHz, CDCl₃/TMS, d/ppm, J/Hz) δ: 7.41 (s, 16H), 5.36 (s, 4H), 3.77 (d, *J* = 12 Hz, 8 H), 3.65 (d, *J* = 8 Hz, 8 H), 1.30 (s, 12H), 0.80 (s, 12H). ESI-MS (+): *m/z* 1000.98 [M+H]⁺.

Synthesis of bis[1,2-di(4-formylphenyl)ethylene-1,2-dithiolate] nickel complex Ni(bded)₂. To a solution of 4 (400 mg, 0.4 mmol) in CHCl₃ (30 mL), trifluoroacetic acid (10 mL) was added, and the green colored solution was stirred at room temperature for 24 h under argon atmosphere. The completion of the reaction was monitored by TLC. On completion, the reaction mixture was diluted with dichloromethane (50 mL) and water (50 mL). The organic layer was separated and washed with saturated aqueous NaHCO₃ solution (3 x 30 mL) and water. The organic layer was separated, dried over anhydrous Na₂SO₄, and evaporated in vacuo. The residue was purified by column chromatography (CH₂Cl₂; silica gel, 200-300 mesh), yielding Ni(bded)₂ (241 mg, 92%) as a green solid. ¹H NMR (400 MHz, CDCl₃/TMS, d/ppm, J/Hz) δ: 10.04 (s, *J* = 8.5 Hz, 4H), 7.83 (d, *J* = 8.0 Hz, 8 H), 7.55 (d, *J* = 8.0 Hz, 8 H). ESI-MS (+): *m/z* 656.44 [M+H]⁺.

Preparation of graphene oxide (GO)

GO was synthesized according to a modified Hummers' method. S1, S2 In a typical

synthesis, 3 g of graphite powder, 2.5 g of $K_2S_2O_8$, 2.5 g of P_2O_5 , and 20 mL of H_2SO_4 were added sequentially to a 50 mL round-bottom flask. The above graphite suspension was then heated to 353 K and stirred for 4 hours. After cooling to room temperature, the graphite suspension was separated by filtration, neutralized with sufficient water, and finally dried at 333 K overnight.

The pre-oxidized graphite powder was placed in a 500 mL round-bottom flask, 120 mL of concentrated sulfuric acid was slowly added and stirred thoroughly, and the temperature was controlled below 303 K with an ice bath. Then, 15 g of $KMnO_4$ was slowly added to the above suspension and it could be seen that the suspension turned dark green. The resulting product was stirred at 328 K for 6 h. The color of the product changed from dark green to dark brown. After cooling to room temperature and the addition of 20 mL of H_2O_2 , the solution immediately turned bright yellow. The above suspension was washed with deionized water until $pH = 7$. Finally, the washed suspension was sonicated for 3 h to obtain a homogeneous GO suspension.

Synthesis of TAP/GO. TAP/GO samples were prepared using a solvothermal synthesis method using synthesized graphene oxide (GO). In a stainless steel reactor, the precursor GO powder (usually 200mg) was mixed with 2,3,6,7-tetra (4-aminophenyl) pyrene (TAP), and methanol (50 mL) was added. Close the reactor under nitrogen and anneal at 90 ° C for different periods: 4-96 hours. Centrifuge the reaction mixture at 4400 rpm for 15 minutes to separate the powder from the remaining methanol solution. Remove unreacted TAP by repeatedly washing with methanol, and finally vacuum dry the sample at room temperature for at least 12 hours

Synthesis of TAP/GO. Similar to the synthesis method of TAP/GO, it only requires replacing TAP with TAPP.

Electrochemical method

The working electrode preparation method: 5 mg of catalyst were dispersed in 40 μ L

Nafion and the mixture of 480 μL water and 480 μL ethanol solution. The appropriate catalyst suspension was coated on a piece of pre-treated carbon paper (CP, $1 \times 2 \text{ cm}$) as a working electrode (loading amount is $1 \text{ mg}\cdot\text{cm}^{-2}$), Hg/HgO (1 M KOH) and Pt electrode were used as reference electrode and counter electrode, respectively.

The electrochemical measurements were all carried out in CHI 660.

Calculations

The equation (1) is used for measuring capacitance by cyclic voltammetry:

$$C_l = \frac{\int_{V_a}^{V_c} I(V) dV}{mv(V_a - V_c)}$$

where m is the mass of the active materials (g), v is the scanrate of C–V curves (V/s); ($V_a - V_c$) represents the potential win-dow (V); I is the discharge current (A).

Whereas equation (2) is used for the calculation of gravimetric capacitance from the chargedischarge method.

$$C_s = \frac{(I \times \Delta t)}{\Delta V * m}$$

Where Δt = Discharge time (Sec) from GCD study, ΔV = Potential window (V); I = Constant current used for charging and discharging (mA) ; m = Active mass of the COF sheet exposed in the electrolyte (mg)

The specific energy (E) and specific power (P) of a supercapacitor against the two electrodes in device were calculated based on the total mass of the active materials using the following equations:

$$E = 1/2 * C * \Delta V^2 / 3600,$$

$$P = E * 3600 / \Delta t,$$

where ΔV is the potential change during the discharge process and Δt is the discharge time.

The conductivity capacitance contributions of the electrode and correlation coefficient fitting curve were calculated by the following equations:

$$\sigma = L\Delta I / R\Delta V$$

$$i = k_1v + k_2v^{1/2}$$

$$i = av^b$$

where i (A) is the peak current, k_1v stands for the capacitive behavior for electrical double-layer capacitance, $k_2v^{1/2}$ represents the diffusion behavior for pseudo-capacitance, v (mV s^{-1}) is the scanning rate, a and b are the correlation coefficient acquired by plotting $\log(i)$ versus $\log(v)$, $b = 0.5$ represents an internal diffusion process with low kinetics, while $b = 1$ refers to an ideal capacitive process with fast kinetics.

The electronic conductivity measurement was carried out by following equations: Typically, the sample was first thoroughly ground and then was placed in a sample holder with a diameter of 1 mm. The sample was clamped between two polished steel sheets and pressed into a pellet using a pneumatic pressure piston at 15 MPa. The electronic conductivity was measured between the top and bottom metallic surfaces of the press holder at 25 °C. The electronic conductivity (σ) of the materials were determined according to the following equation:

$$\sigma = l/(R \cdot A)$$

where σ (mS cm^{-1}) is the conductivity, L (cm) is the thickness, S (cm^2) is the area, ΔI (A) and ΔV (V) is the polarisation current and potential

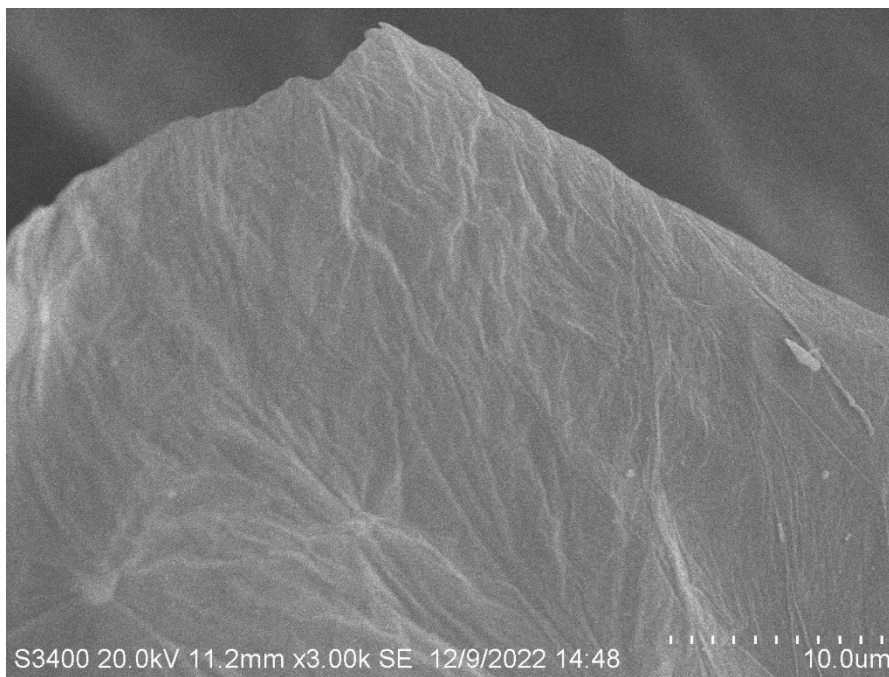


Figure S1. SEM image of GO.

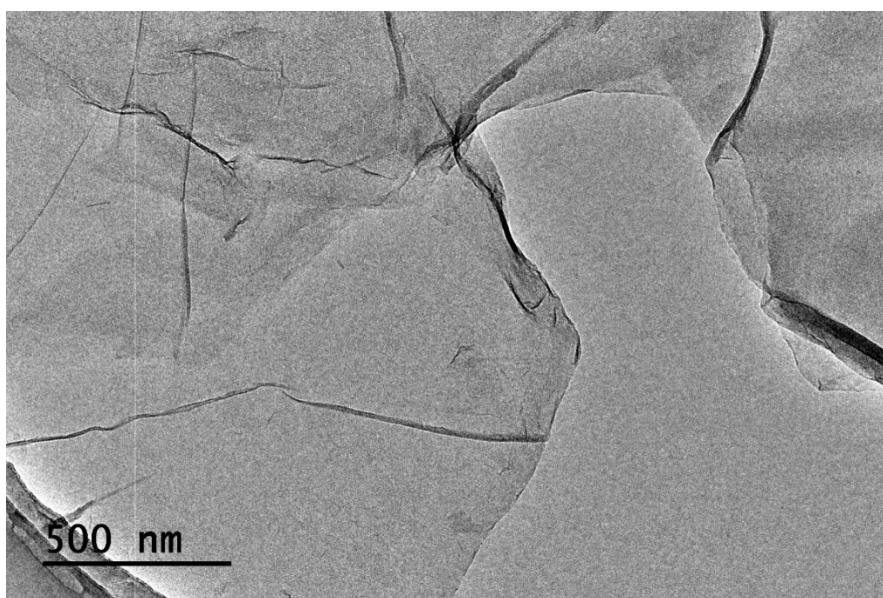


Figure S2. TEM image of GO.

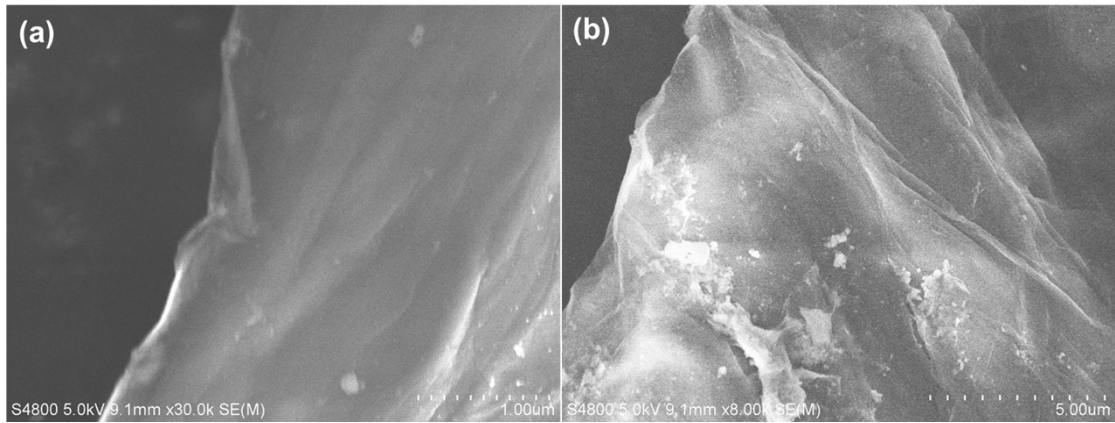


Figure S3. SEM images of TAP-GO and TAPP-GO.

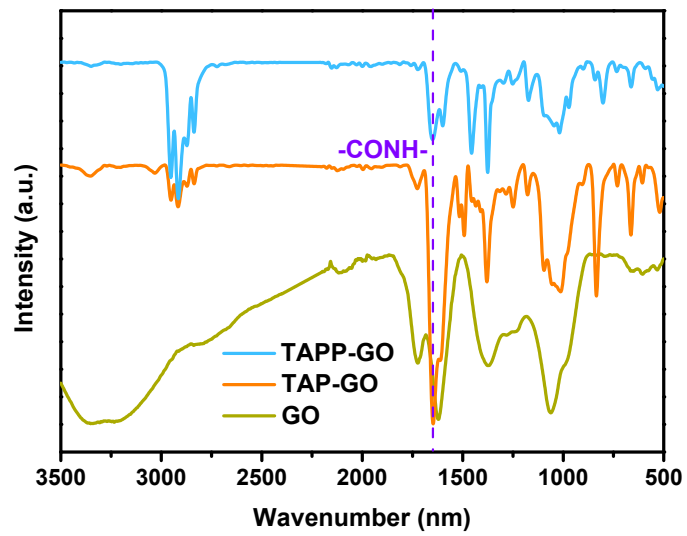


Figure S4. FTIR spectrum of GO, TAP-GO, and TAPP-GO.

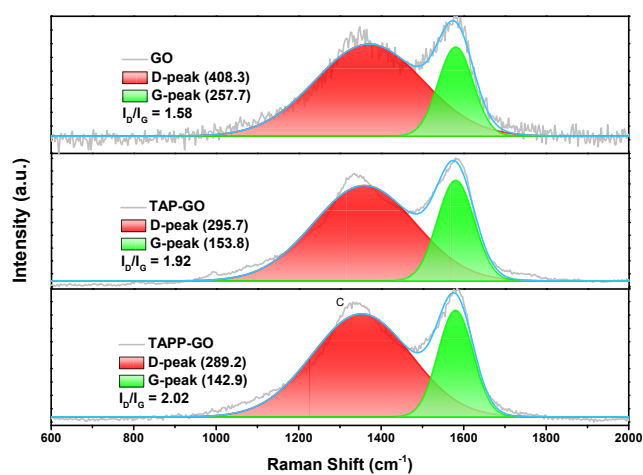


Figure S5. Raman spectrum of GO, TAP-GO, and TAPP-GO.

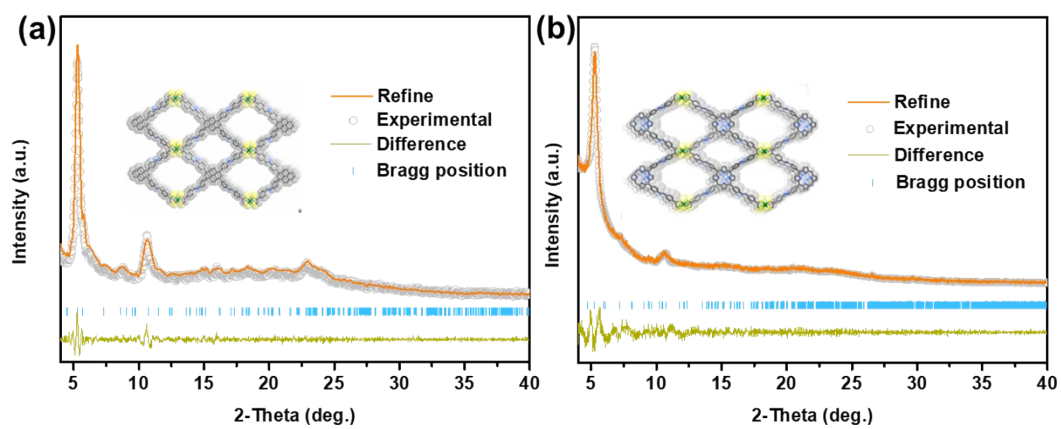


Figure S6. Structural characterization of Ni-TAP and Ni-TAPP. PXRD patterns of (a) Ni-TAP and (b) Ni-TAPP.

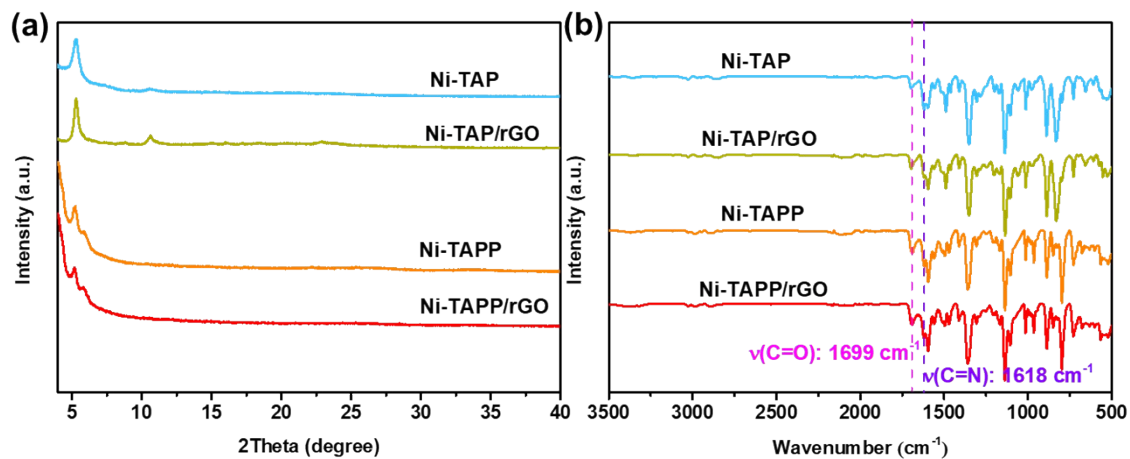


Figure S7. Structural characterization of Ni-TAP, Ni-TAP/rGO, Ni-TAPP, Ni-TAPP/rGO. (a) PXRD patterns, (b) FTIR spectra.

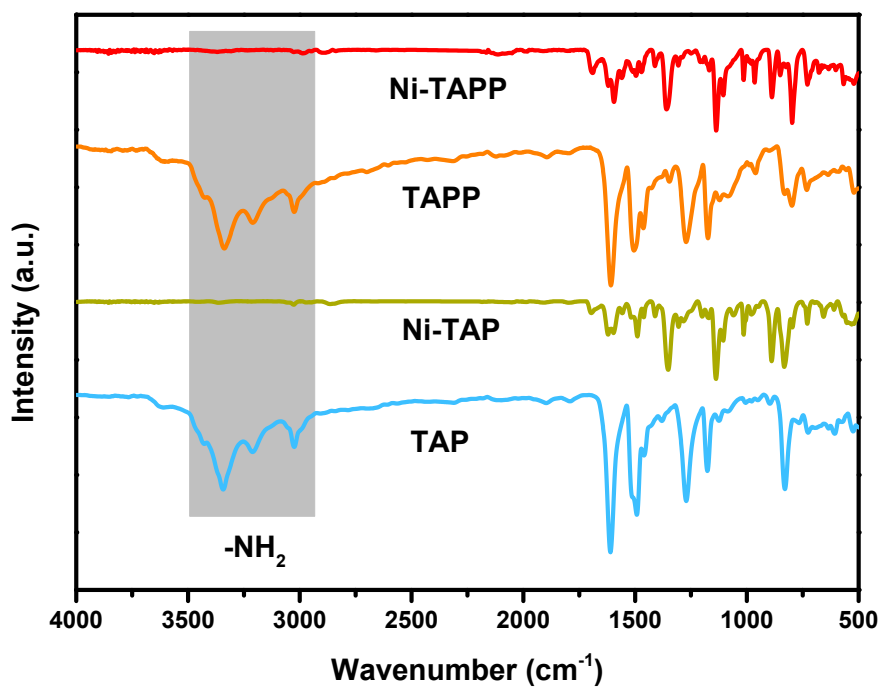


Figure S8. FTIR spectra of Ni-TAPP, TAPP, Ni-TAP, and TAP.

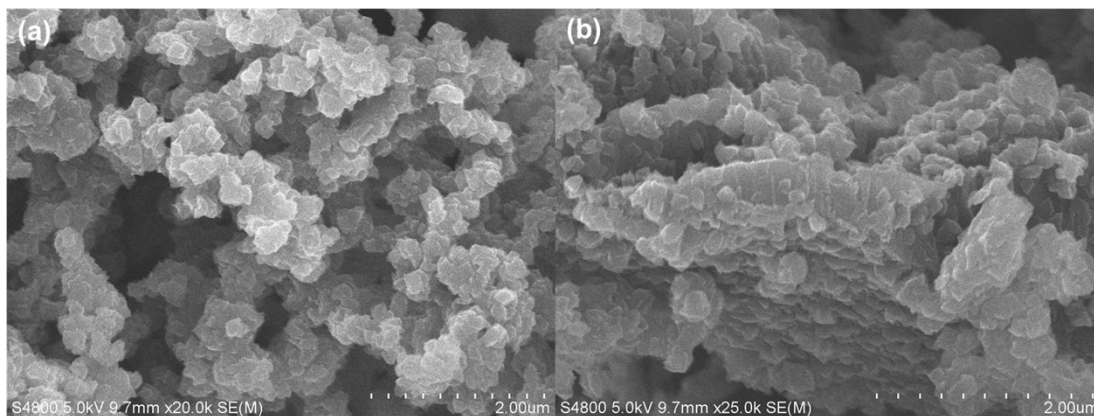


Figure S9. SEM images of Ni-TAP, Ni-TAPP.

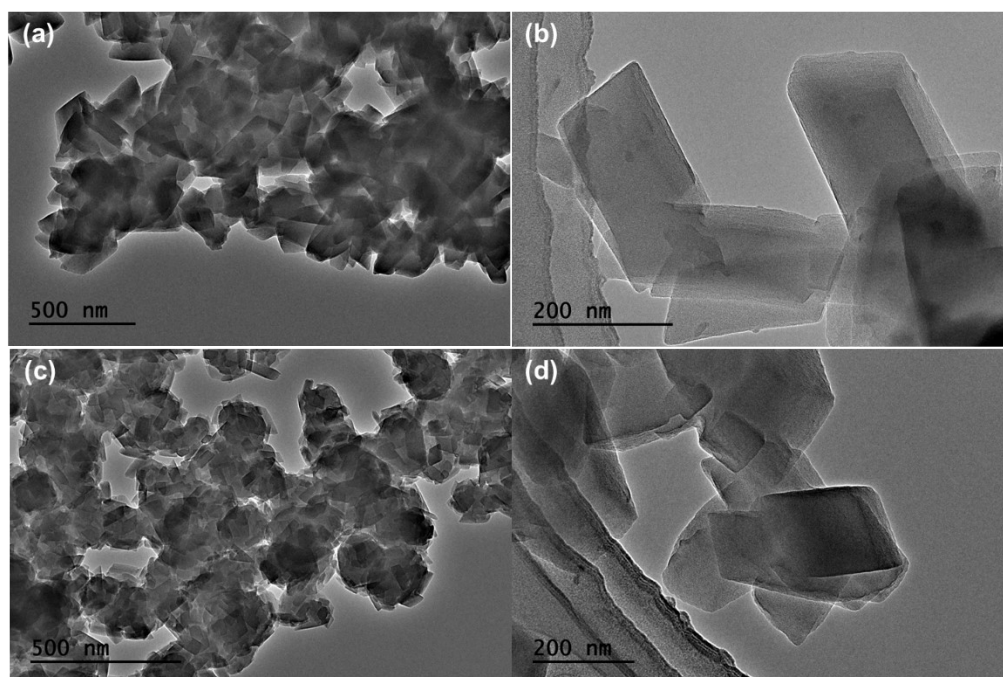


Figure S10. TEM images of Ni-TAP, Ni-TAPP.

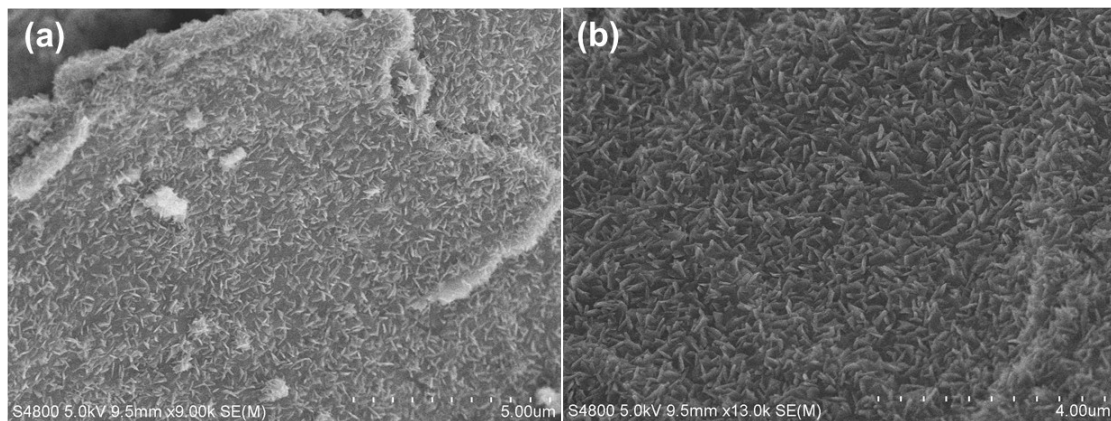


Figure S11. SEM images of Ni-TAP/rGO, Ni-TAPP/rGO.

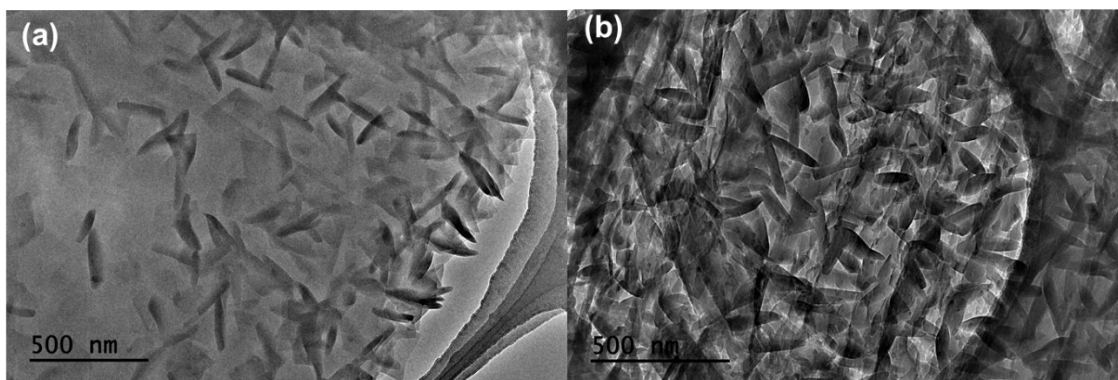


Figure S12. TEM images of Ni-TAP/rGO, Ni-TAPP/rGO.

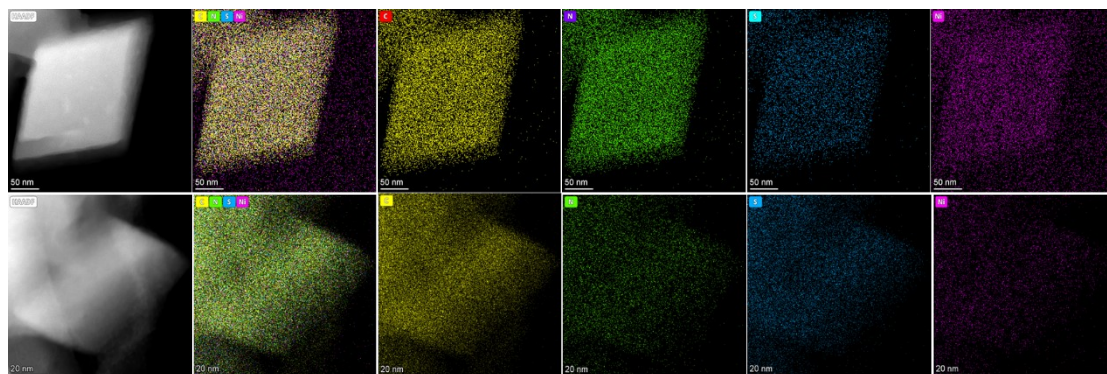


Figure S13. TEM mapping of Ni-TAP, Ni-TAPP.

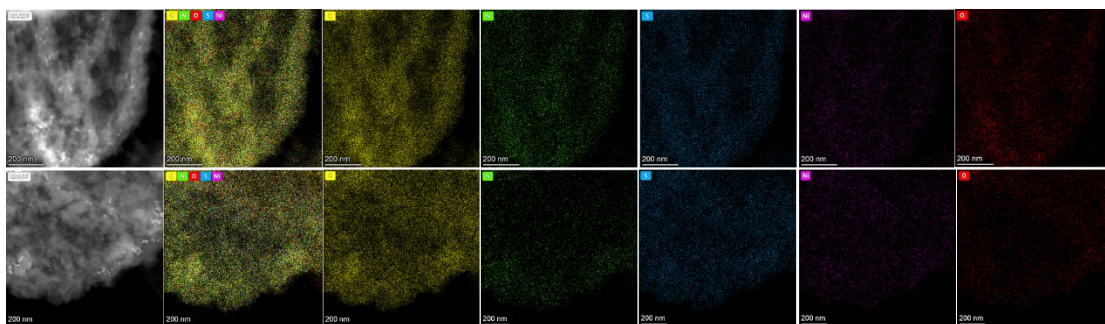


Figure S14. TEM mapping of Ni-TAP/rGO, Ni-TAPP/rGO.

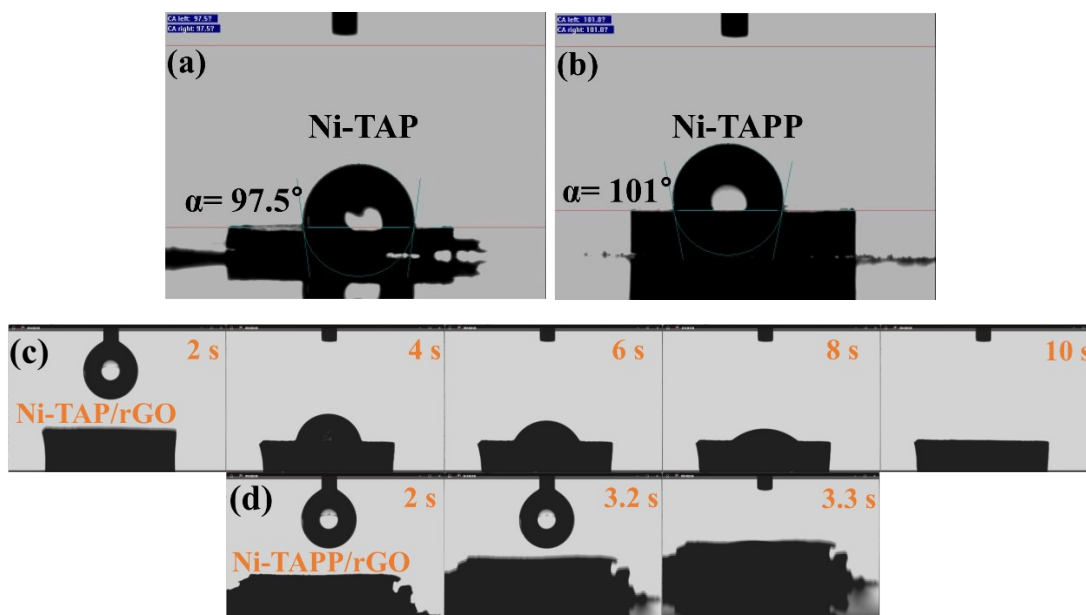


Figure S15. Contact angles of the water drop on (a) Ni-TAP, and Ni-TAPP; (b) Ni-TAP/rGO, and Ni-TAPP/rGO.

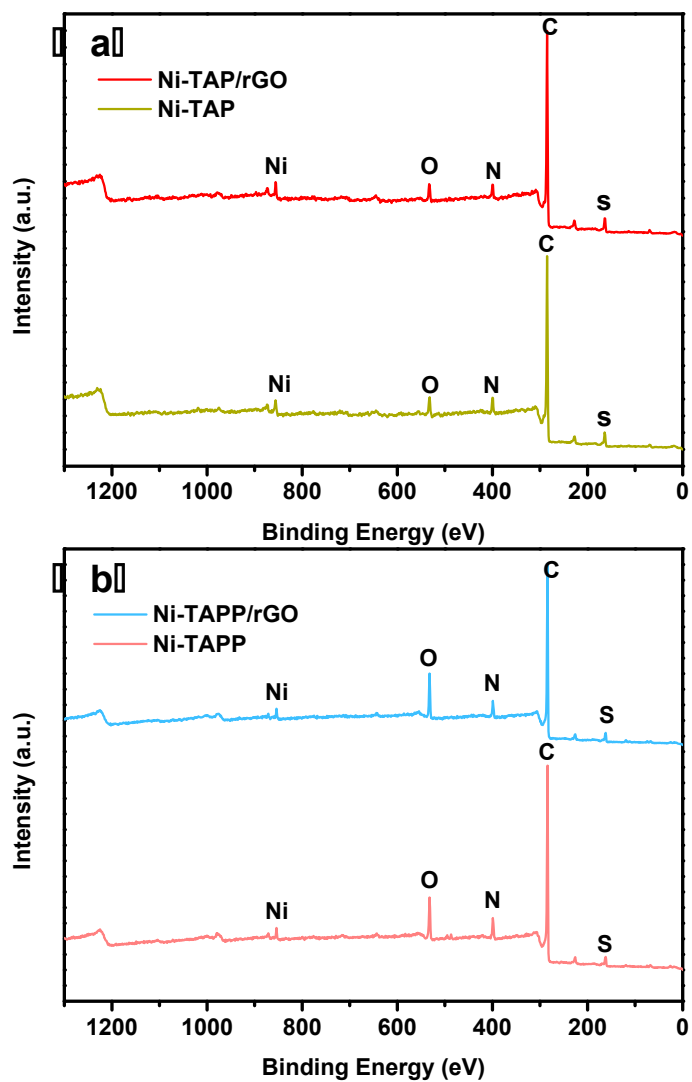


Figure S16. XPS survey spectra.

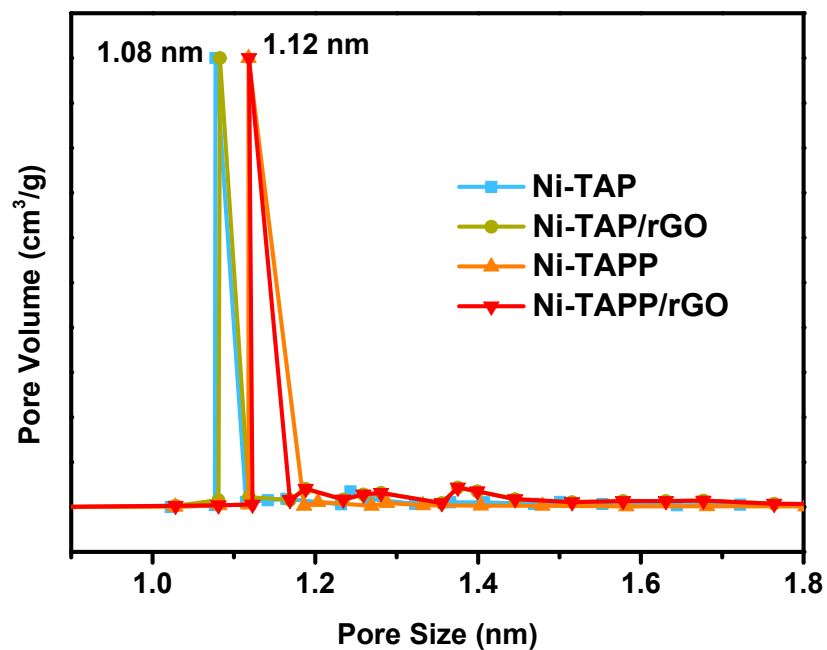


Figure S17. Pore size distribution of Ni-TAP, Ni-TAP/rGO, Ni-TAPP, and Ni-TAPP/rGO.

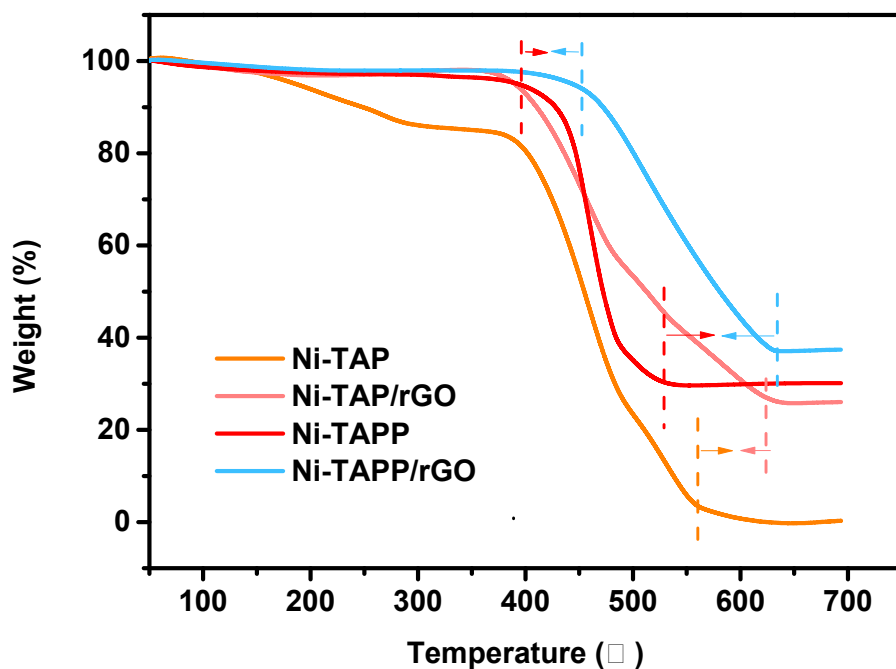


Figure S18. The thermogravimetric analysis of different samples.

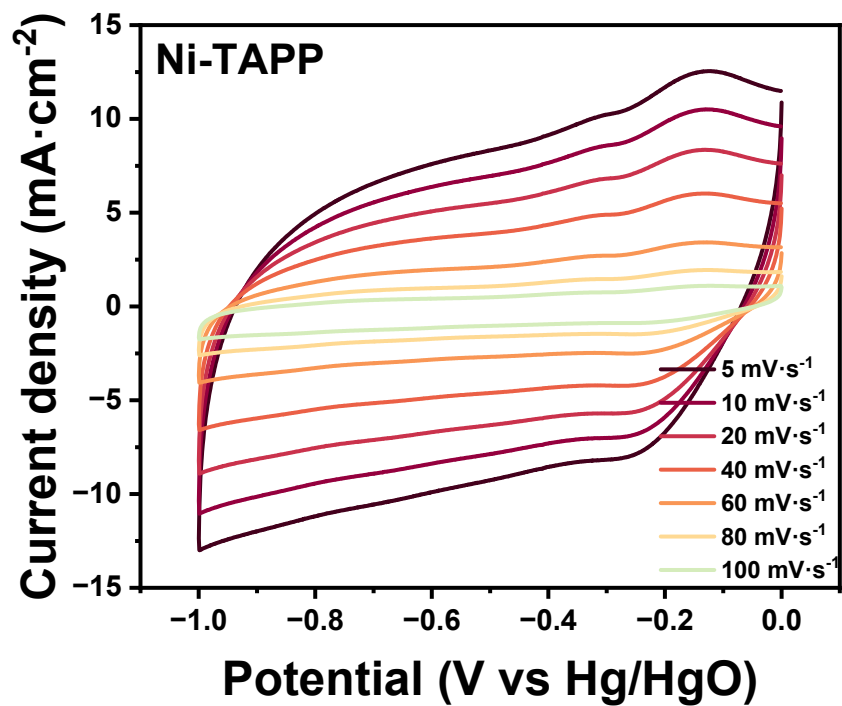


Figure S19. The CV curves of Ni-TAPP at various scan rates from 5~100 mV s^{-1} .

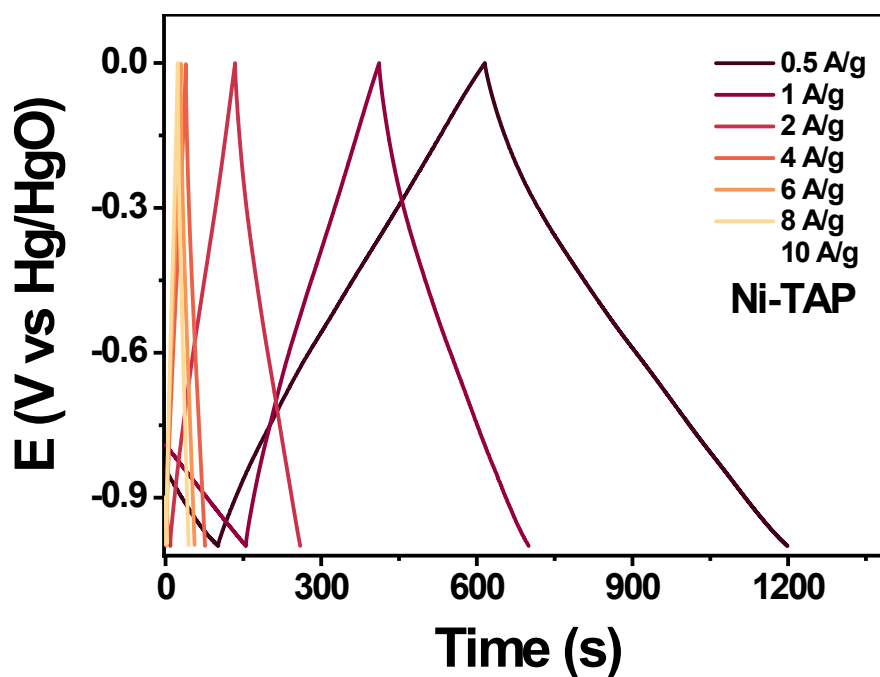


Figure S20. The GCD profiles at different current densities from 0.5~10 A g^{-1} .

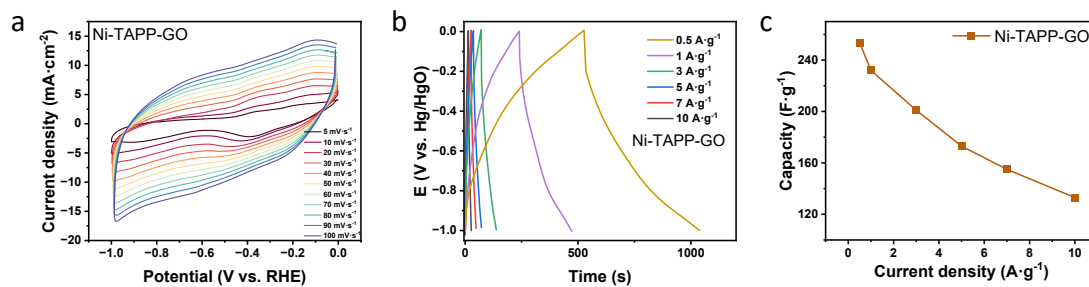


Figure S21. Electrochemical performance of Ni-TAPP-GO in 6 M KOH electrolyte: a) CV curves of Ni-TAPP-GO at various scan rates from 5~100 mV s⁻¹; b) The GCD profiles of Ni-TAPP-GO at different current densities from 0.5~10 A·g⁻¹; c) Comparison of specific capacitance at current densities of 0.5~100 A·g⁻¹

e

For Ni-TAPP-GO, during cyclic voltammetry (CV) analysis (Figure S), the scan rate was set from 5 mV·s⁻¹ to a maximum of 100 mV·s⁻¹. The CV profiles feature a quasi-rectangular shape even at an ultrahigh scanning rate of 100 mV·s⁻¹, indicating the capability as well as the ideal electric double-layer capacitance (EDLC) behavior. The symmetry-shaped GCD profiles of Ni-TAPP-GO at 0.5–10 A g⁻¹ are shown in Figure S, showing a specific capacitance (C_g) of 253.7 F·g⁻¹ at a current loading of 0.5 A·g⁻¹, and rate capability with 52.4% capacitance retention at 0.5–10 A·g⁻¹.

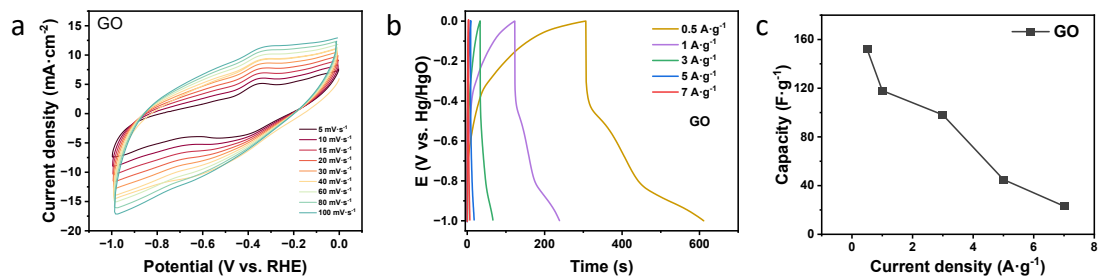


Figure S22. Electrochemical performance of GO the in 6 M KOH electrolyte: a) CV curves of GO at various scan rates from 5~100 mV s^{-1} ; b) The GCD profiles of GO at different current densities from 0.5~10 A g^{-1} ; c) Comparison of specific capacitance at current densities of 0.5~100 A g^{-1}

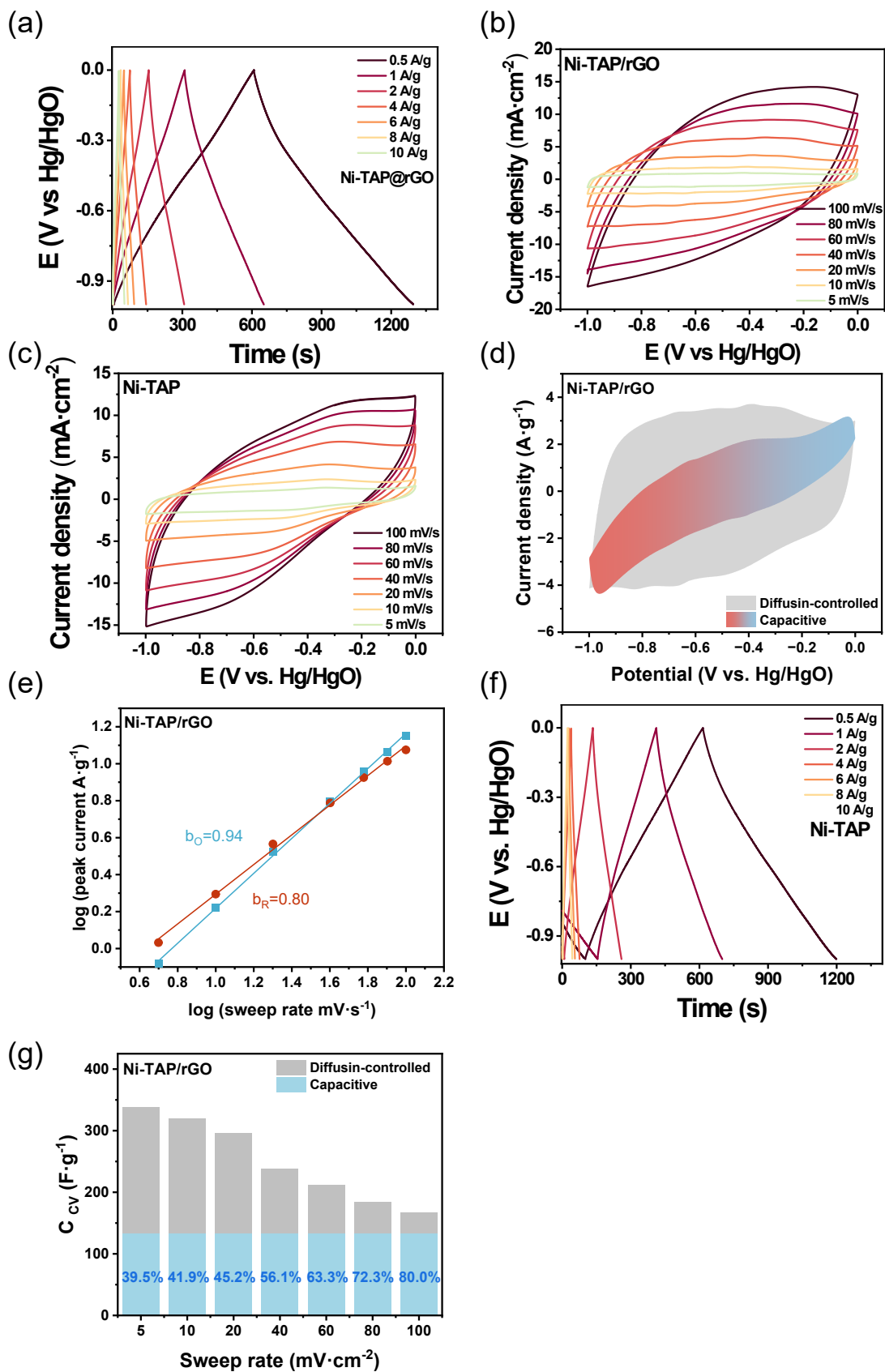


Figure S23. Electrochemical performance of Ni-TAP and Ni TAP/rGO the in 6 M KOH electrolyte: a) CV curves of Ni-TAP/rGO at various scan rates from 5~100 mV s^{-1} ; b)The GCD

profiles of Ni-TAP/rGO at different current densities from 0.5~10 A·g⁻¹; c) CV curves of Ni-TAP at various scan rates from 5~100 mV s⁻¹, d)The GCD profiles of Ni-TAP at different current densities from 0.5~10 A·g⁻¹; e) The fitting plot between log(i) and log(v), f) CV curves with the diffusion contribution at 20 mV s⁻¹, g) normalized diffusion contribution at various scan rates.

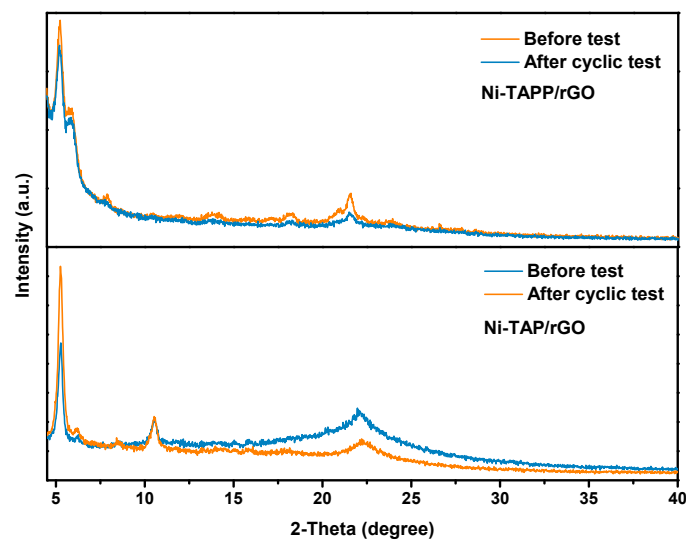


Figure S24. XRD pattern of Ni-TAP/rGO, and Ni-TAPP/rGO fresh prepared and after 1000 cyclic test.

Table S1. H₂-TPD of different samples.

sample	Metal dispersion
Ni-TAP	0.051%
Ni-TAP/rGO	0.068%
Ni-TAPP	0.049%
Ni-TAPP/rGO	0.077%

Table S2. Comparison of specific capacitance performance with Ni-TAPP/rGO, Ni-TAP/rGO and other materials.

Materials	Energy storage performance (F g ⁻¹)	Refs.
Ni-TAPP/rGO	367.5	<i>This work</i>
Ni-TAP/rGO	346	<i>This work</i>
c-PAN@MCA _{0.25}	338.6	<i>J. Mater. Chem. A</i> , 2024, 12 , 6712-6723
NH ₂ -TMU-53	325	<i>ACS Appl. Mater. Interfaces</i> 2019, 11 , 14759–14773
PCNS	310	<i>Nano Energy</i> 2016, 27 , 377-389.
COF/rGO	269	<i>Nat. Commun.</i> 2020, 11 , 4712.
COF@OHP	249	<i>Chem. Eng. J.</i> 2020, 387 , 124071.
Ni ₃ (BHT) ₂	245	<i>J. Am. Chem. Soc.</i> 2021, 143 , 2285.
Cu ₃ (HHTP) ₂	240	<i>Chem. Sci.</i> 2022, 13 , 9210.
Cu-CAT NWAs	202	<i>Adv. Funct. Mater.</i> 2017, 27 , 1702067.
Cu-HAB	215	<i>Nat. Energy</i> 2018, 3 , 30.
Ni-pPDA//GC	184.7	<i>Chem. Eng. J.</i> 2019, 361 , 1235–1244.
TpOMe-DAQ	169	<i>J. Am. Chem. Soc.</i> 2018, 140 , 10941–10945
CNF@Ni-HITP	141	<i>ACS Nano</i> 2019, 13 , 9578.
DAB/GCF	129.2	<i>Chem. Eng. J.</i> 2022, 449 , 137858.
Ni ₃ (HITP) ₂	111	<i>Nat. Mater.</i> 2020, 19 , 552
Cu ₃ (THQ) ₂	32	<i>ACS Nano</i> 2022, 16 , 3145.